[논문] 한국소성·가공학회지, 제 32 권 제 5 호, 2023
Transactions of Materials Processing, Vol.32, No.5, 2023
http://data.doi.or.kr/10.5228/KSTP.2023.32.5.268

다단 성형 공정 시 고-Mn 강의 타원형 용기 헤드에서의 변형률 분포: 유한요소해석

Preetham Alluri[1] · Lalit Kaushik[2] · 최시훈[3,#]

Strain Evolution in High-Mn Steel Ellipsoidal Vessel Head during Multi-forming Process: A Finite Element Analysis

Preetham Alluri, Lalit Kaushik, and Shi-Hoon Choi
(Received July 22, 2023 / Revised August 17, 2023 / Accepted September 13, 2023)

Abstract

ISO 21029 cryogenic vessel is used to transport cryogenic fluids. High-manganese steel (High-Mn steel) is widely regarded as suitable for use at cryogenic temperatures. The conventional way of manufacturing an ellipsoidal vessel head involves incremental stretching, followed by a spinning process. In this study, an alternative method for forming an ellipsoidal vessel head was proposed. Finite element analysis (FEA) was used to theoretically examine the strain evolution during a multi-stage forming process, which involved progressive stretching, deep drawing, and spinning of High-Mn steel. The distribution of effective strain and strain components were analyzed at different regions of the formed part. The FEA results revealed that only normal strains were evident in the dished region of the vessel head due to the stretching process. However, the flange region experienced complex strain evolution during the subsequent deep drawing and spinning process.

Keywords : High-Mn steel, Cryogenic vessel, Ellipsoidal head, Stretching, Deep drawing, Metal spinning

1. Introduction

High-manganese steel (High-Mn steel) is a type of austenitic steel with a Mn content greater than 20%. Its excellent mechanical properties of high strength and ductility have led to growing interest in using High-Mn steel[1]. High-Mn steel has shown to be effective for cryogenic applications due to its outstanding cryogenic temperature properties[2-4]. As industries and transport sectors increasingly use cryogenic fluids, the storage and transportation of these fluids present challenges due to their low temperatures.

Cryogenic vessels that conform to the standards of ISO 21029 are used to store cryogenic fluids[5]. The vessel head, as an end closure, is a key component of the vessel. There are various kinds of vessel heads with different geometry, but, the current studies has focused on the 2:1 ellipsoidal head[5]. Zheng et al. conducted a comprehensive study on the numerical analysis of the stamping of various ellipsoidal head dimensions and concluded that the optimal parameter for describing deformation during head stamping was equivalent plastic strain[6]. They also analyzed the strain distribution along the cross-sectional profile of the deformed head. Soltani et al. used finite element analysis (FEA) to investigate dimensional deviations at different zones of ellipsoidal steel heads during deep drawing[7]. They concluded that the maximum

1. 순천대학교 첨단부품소재공학과, 박사과정
2. 순천대학교 첨단부품소재공학과, 박사후 연구원
3. 순천대학교 첨단부품소재공학과, 교수
#Corresponding Author: Department of Advanced Components and Materials Engineering, Suncheon National University
E-mail: shihoon@scnu.ac.kr, ORCID: 0000-0002-2557-0646

Table 1 Chemical composition

C	Mn	Si	Cr	Fe/others
0.32	24	0.014	3.62	Balance

thinning occurs at the junction of the knuckle and the straight flange region. Zhang et al. employed FEA modeling to understand the stress and strain distribution during power spinning of ellipsoidal heads with variable thickness and validated the results experimentally[8]. It is well known that residual stresses are generally observed in the cold formed components which can affect the subsequent processes and overall life span of the product[9]. M.S. Ragab et al. concluded that residual stresses in deep drawn cups can be significantly reduced by implementing ironing process[10]. Y.C. Lin et al. made an attempt to reduce the residual stresses by annealing treatment on the spun ellipsoidal head and studied the residual-stress relaxation mechanism[11]. Some industries utilize incremental stretching to form the hemispherical part of the ellipsoidal head before employing the spinning process to achieve the straight flange and desired geometry. In this case, the workpiece is expected to undergo a significant plastic deformation and a complex strain path.

In the present study, to suggest an alternating manufacturing process, FEA was employed to investigate the strain development in High-Mn Steel during the sequential stages of stretching, deep drawing, and spinning, which together form an ellipsoidal vessel head.

2. Experimental details

The present study was conducted on hot-rolled High-Mn steel, with its chemical composition detailed in Table 1. In this research, a Finite Element Analysis (FEA) tool was utilized to examine the strain development throughout the consecutive processes of stretching, deep drawing, and spinning, resulting in the formation of an ellipsoidal vessel head.

2.1 Head forming procedure.

Fig. 1(a) shows a typical ISO 21029 ellipsoidal vessel head, and Fig. 1(b) illustrates the cross-section view of the

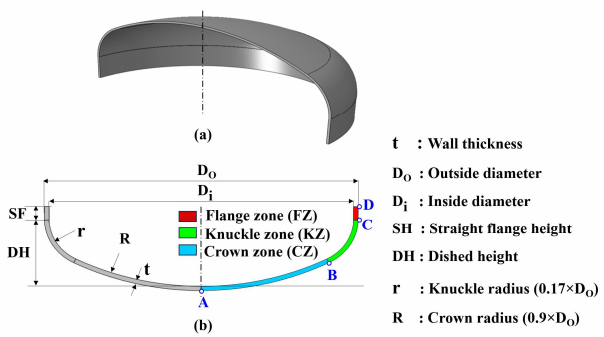

Fig. 1 (a) 3D view of an ISO 21029 ellipsoidal vessel head; (b) Cross-section view of the ellipsoidal vessel head and its geometry specifications

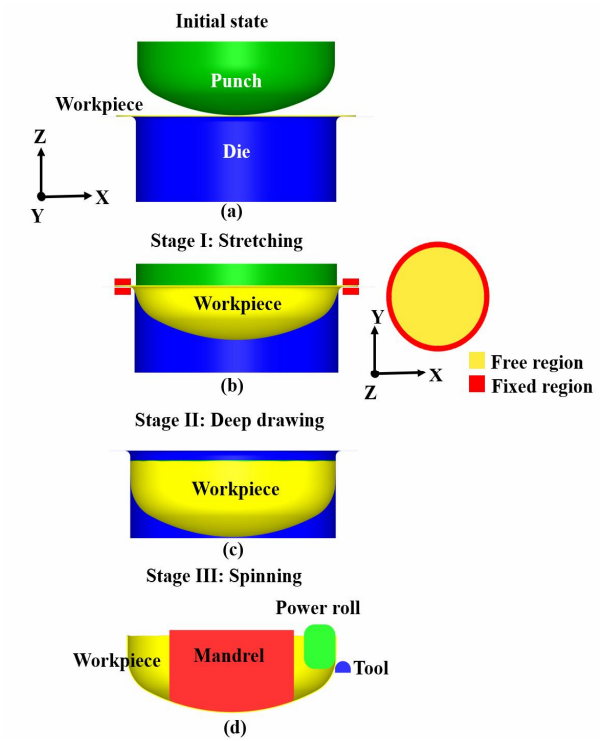

Fig. 2 Schematic view of (a) Initial state; (b) Stretching process; (c) Deep drawing process; (d) Spinning process

ellipsoidal head along with its specifications. The ellipsoidal head can be divided into three regions: Crown zone (CZ), Knuckle zone (KZ), and Flange zone (FZ), as highlighted in Fig. 1(b). The CZ and KZ regions together form dish region. Fig. 2 depicts the proposed multi-stage forming process for the ellipsoidal vessel head. Fig. 2(a) represents the initial state of the forming process. Fig. 2(b) demonstrates stretching process, during which the

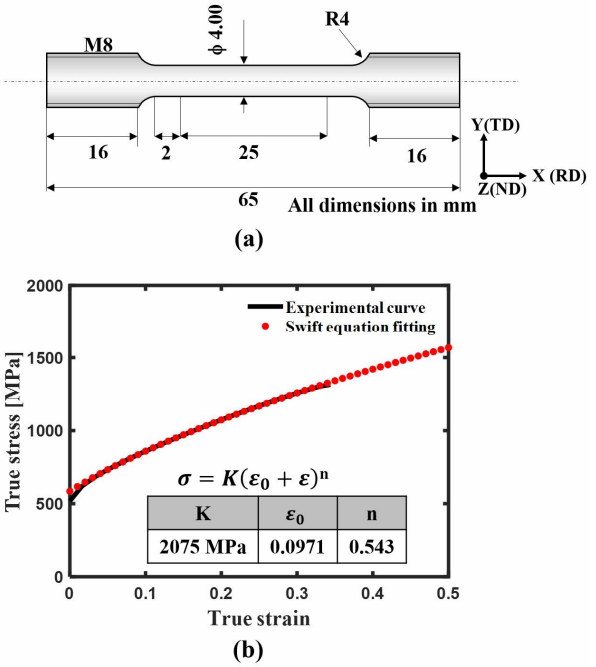

Fig. 3 (a) Uniaxial tensile test specimen geometry; (b) True stress-plastic strain data obtained from uniaxial tensile test and Swift equation fitting curve and parameters

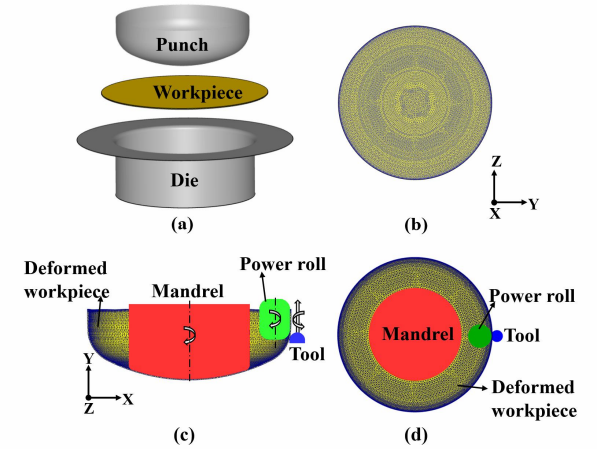

Fig. 4 (a) Initial FEA set-up for stretching and deep drawing process; (b) Initial mesh condition of the workpiece; (c) and (d) FEA set up for spinning process in different views

workpiece is clamped along its periphery and plastically deformed by the punch to create the dish region. Fig. 2(c) presents the deep drawing process, where the grip on the workpiece periphery is released, and the punch is further lowered to form the flange region.

The thickness distribution in the flange region might be heterogenous due to wrinkles generated during the deep drawing process. Fig. 2(d) depicts the spinning process, which is performed to eliminate the effect of wrinkles on the flange region and achieve the final geometry of the head.

2.2 Uniaxial tensile test

Uniaxial tensile tests were carried out to determine the material's mechanical properties, which were then utilized in the FEA. Fig. 3(a) shows the geometry of the round bar specimen used for the tensile tests. The samples were cut along the rolling direction using wire electrical discharge machining (EDM). The tensile tests were conducted at room temperature (RT) at a strain rate of 0.7/sec. Fig. 3(b) shows the true stress-true plastic strain data obtained from the tensile tests. This data was fitted using the classical constitutive Swift equation and used as a flow property for the workpiece in the simulation[12]. The fitted parameters are mentioned in Fig. 3(b).

3. Simulation details

A continuum element-based 3D FEA simulation was carried out using DEFORM v12.0 software to investigate the strain evolution during the ellipsoidal head forming process. The stretching and deep drawing model consisted of a punch, die, and workpiece. The punch and die were assumed as rigid parts, while the workpiece was modeled as a rigid-plastic body assuming isotropic behavior. Fig. 4(b) displays the tetrahedral mesh of the workpiece, consisting of 115,181 elements. Throughout the stretching process, the workpiece's linear movements at its periphery were constrained in the X, Y, and Z directions.

The punch was allowed to move exclusively in the Z direction at a velocity of 10 mm/s for a displacement of 495 mm. During the deep drawing stage, constraints on the workpiece's periphery were removed, and the punch movement continued until the flange shape was achieved. Figs. 4(c) and (d) illustrate the spinning process assembly, which includes the deformed workpiece, mandrel, power roll, and tool. The mandrel functioned to rotate the

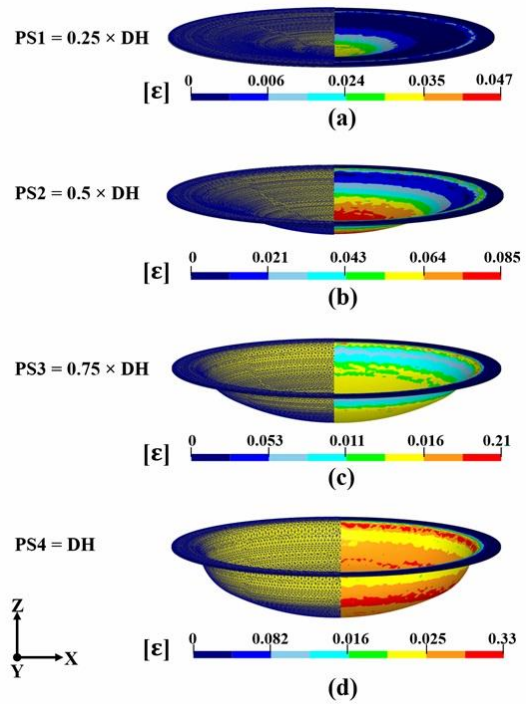

Fig. 5 (a)-(d) Effective strain distribution of the deformed part during stretching process at different punch strokes

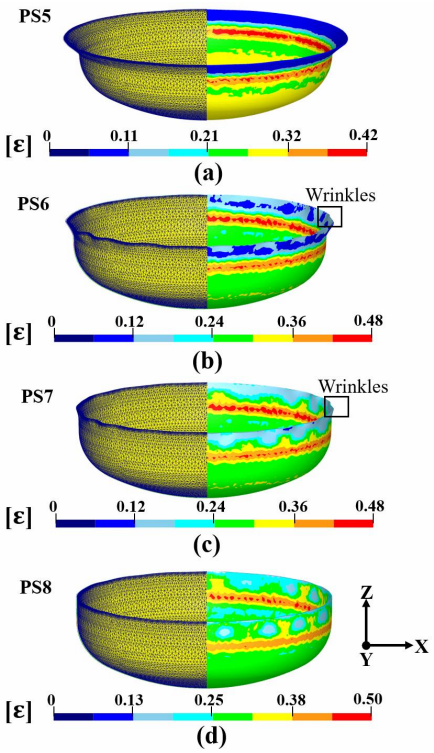

Fig. 6 (a)-(d) Effective strain distribution of the deformed part during deep drawing process at different punch strokes

deformed workpiece by implementing a sticking contact condition. The power roll, whose rotation axis is its Z axis, was in contact with the inner surface of the deformed part. The tool was initially positioned at the beginning of the flange region (C) and completed the flange (D) by following a designated tool path. The X, Y, and Z coordinates were determined based on the final head geometry's outer diameter and incorporated into the tool path as a time-dependent function. Moreover, the tool was given rotational motion around its Z axis. A feed rate of 30 rpm was assumed for the mandrel, power roll, and tool, and a friction coefficient of 0.12 was applied between the mating surfaces.

4. Results and discussions

In this section, we discuss the strain evolution in the CZ and KZ regions using the stretching and deep drawing process results, while the spinning results are used to examine the strain distribution in the FZ region.

Fig. 5 illustrates the distribution of effective strain (ε) during the stretching process at various punch strokes (PS). Fig. 5(a) displays the effective strain at PS1, where noticeable effective strain occurs only in the contact region between the punch and workpiece. Strain localization is apparent in the peripheral region due to restricted material flow. Fig. 5(b) depicts the effective strain at PS2, where the maximum effective strain is at the center region, gradually decreasing to zero towards the periphery. Moreover, the strain localization value in the peripheral region has increased. Fig. 5(c) presents the effective strain distribution at PS3, where the punch's contact region with the workpiece exhibits a uniform distribution of effective strain. Fig. 5(d) reveals the final stage of stretching, characterized by a uniform strain distribution throughout the dish region, except at point B, where the punch's radius of curvature changed. Strain localization occurs along the peripheral region, with a maximum effective strain reaching a value of 0.33.

Fig. 6 illustrates the effective strain distribution during the deep drawing process at various intervals. Fig. 6(a)

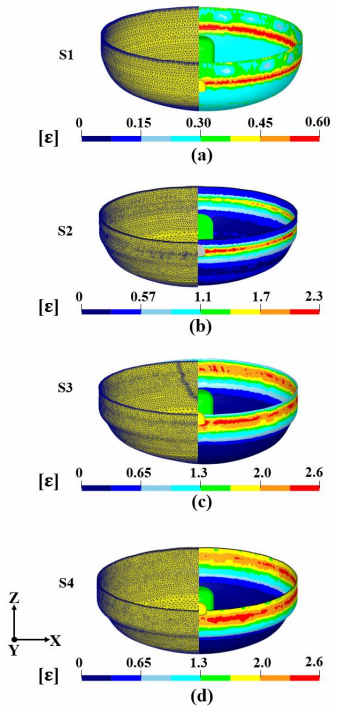

Fig. 7 (a)-(d) Effective strain distribution of the deformed part during spinning process at different stages.

displays the flow of flange material into the die opening as the punch progresses, with the maximum effective strain increasing to 0.42. Figs. 6(b) and (c) reveal wrinkles in the flange region, as there is no blank holder to restrain them. These wrinkles cause a heterogeneous effective strain distribution in the flange region. Fig. 6(d) represents the final formed shape after the deep drawing process, with the inner surface exhibiting a maximum effective strain of 0.5 at the end of the deep drawing process. Figs. 7(a)-(d) demonstrates the effective strain distribution during the spinning process at various intervals. As the tool moves, the effective strain begins to increase, reaching a maximum value of 2.6 at the end of the process. The strain distribution in the flange region is not homogeneous. The outer surface undergoes more extensive strain than the inner surface due to the intense deformation caused by the tool's rotation and vertical translation.

To quantitatively understand the strain evolution along the cross-sectional line profile (A-B-C-D), we plotted the effective strain and strain components on the deformed part after the stretching, deep drawing, and spinning processes.

Fig. 8(a) displays the effective strain line profile during the stretching process, where a uniform effective strain distribution in the CZ region (A-B) is followed by a slight decrease in the KZ region as it approaches point C. This may be because the CZ region had stronger contact with the punch compared to the KZ region. The effective strain exhibits a small spike at point C due to strain localization resulting from the material flow restriction in the FZ region. Fig. 8(b) shows the effective strain line profile illustrating the effective strain distribution after the deep drawing process. The CZ and KZ regions display a similar profile as in the stretching process because of the free flow of material from the FZ region. The effective strain reaches a maximum value of 0.40 at point C due to the wrinkles' impact on the existing strain localization. The FZ region exhibits an effective strain value of ~0.26, similar to the CZ region. Fig. 8(c) presents the effective strain line profile in the FZ region (C-D) after the spinning process. High effective strain is evident in the FZ region, with values increasing from 1.15 at point C and reaching a maximum value of 2.45 before decreasing to 1.92 at the end of the flange path D. Fig. 9(a) displays the strain components line profile after the stretching process. It is evident that all three normal strain components are active, while none of the shear strain components are active in the CZ and KZ zones during the stretching process. Longitudinal strain (ε_{XX}) and transverse strain (ε_{YY}) are tensile in nature, while thickness strain (ε_{ZZ}) is compressive, indicating the thinning phenomenon in this region. The material in the dished area experiences biaxial tensile stress due to the action of the punch in the stretching process. In the CZ region, longitudinal strain (ε_{XX}) maintains a constant value of 0.13 and then exhibits a slightly higher value in the KZ. The transverse strain (ε_{YY}) remains a constant value of 0.13 throughout the CZ region and then linearly decreased to 0 at the end of KZ region. The thickness strain (ε_{ZZ}) has a fluctuating value of around −0.28 in the CS zone and then gradually diminished to −0.20 at the end of the KZ zone path. Fig. 9(b) shows the strain components line profile after the deep drawing process. The strain components in the CZ and KZ regions demonstrate similar behavior as during the stretching process. The tensile nature of longitudinal strain (ε_{XX}) decreases as it reaches the end of

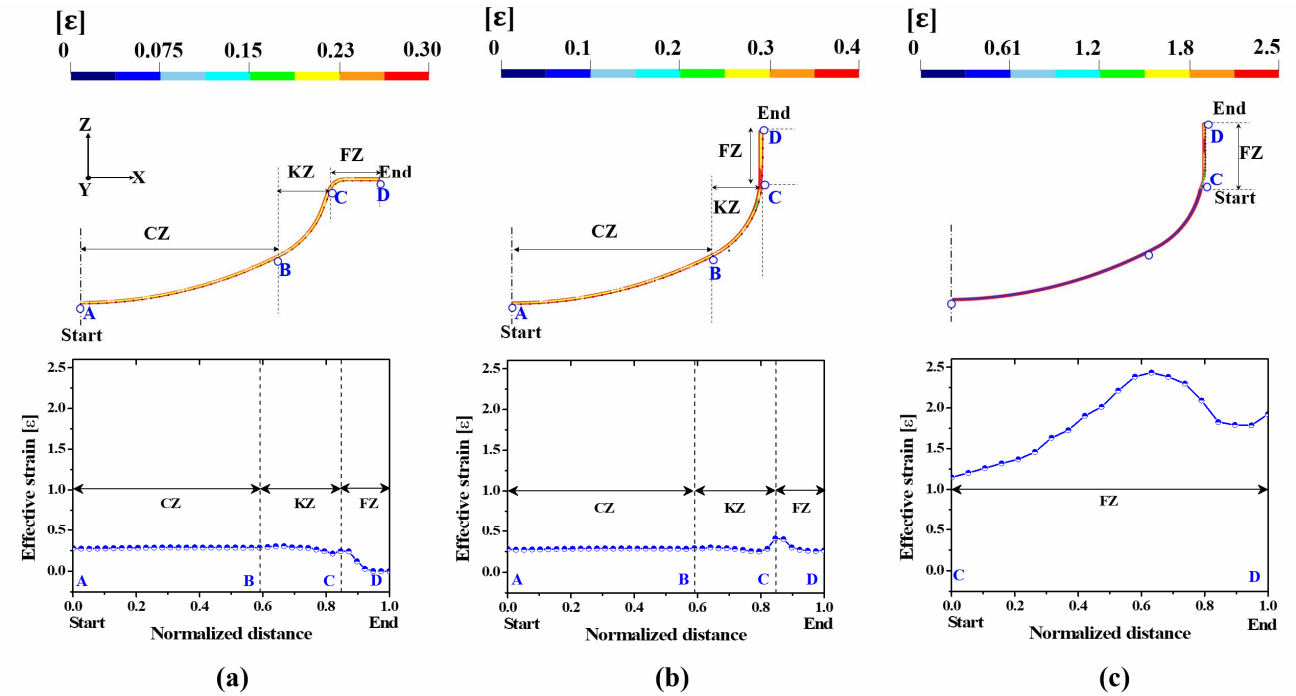

Fig. 8 Effective strain line profile on the deformed part after: (a) stretching process; (b) deep drawing process; (c) spinning process

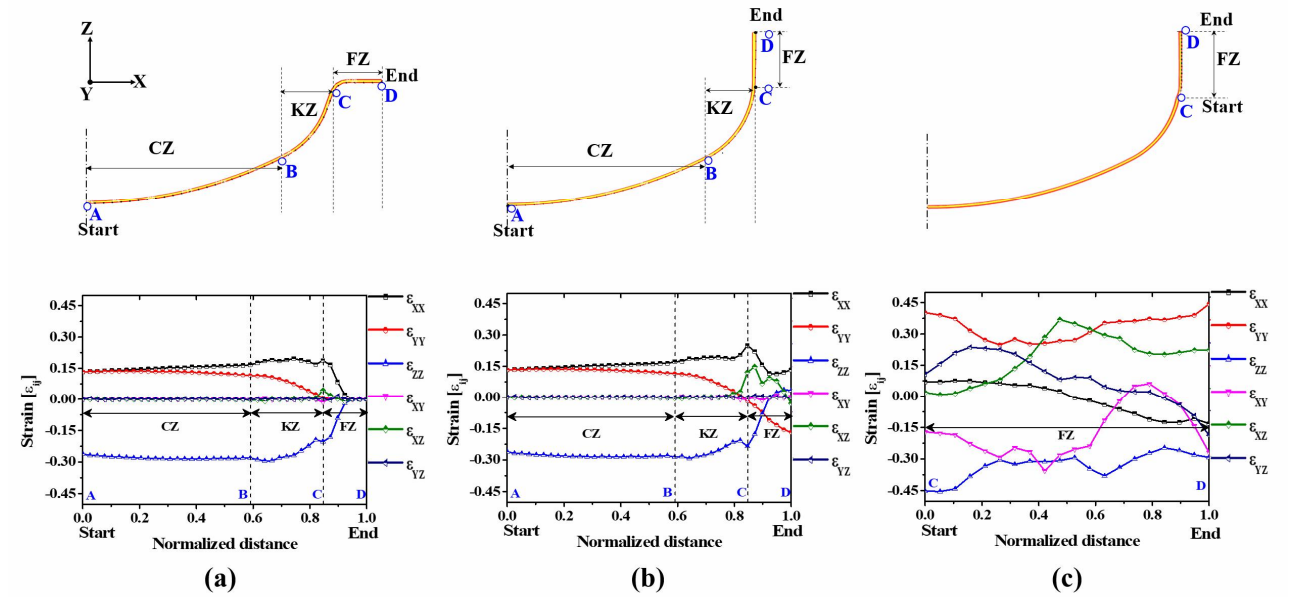

Fig. 9 Strain components line profile on the deformed part after (a) stretching process; (b) deep drawing process; (c) spinning process

the flange in FZ region. The transverse strain (ε_{YY}), which was tensile in the CZ and KZ regions, transitions to a compressive nature in the FZ region. The thickness strain (ε_{ZZ}), which was compressive in the CZ and KZ region, transitions to tensile behavior at the end of the FZ zone. The end part of the FZ region exhibits a thickening phenomenon. Fig. 9(c) presents the strain components line profile of the FZ region after the spinning process. A

complex strain evolution is evident in the FZ region, where all the strain components are active. The longitudinal strain (ε_{XX}) exhibits tensile behavior at the beginning of the flange path, C, and then gradually shifts to compressive behavior. The transverse strain (ε_{YY}) maintains a tensile nature throughout the path. The compressive nature of the thickness strain (ε_{ZZ}) indicates that material experienced thinning in flange region. The shear strain components display erratic behavior.

5. Conclusion

The following conclusions were drawn after theoretically examining the strain evolution in High-Mn steel ellipsoidal vessel head during the sequential stretching, deep drawing, and spinning process using FEA:

A maximum effective strain of 0.33 was experienced by the deformed part after stretching process. The cross-sectional line profile on the deformed part revealed that only normal strain components were active in the CZ and KZ zones. The compressive nature of the thickness strain (ε_{ZZ}) in the CZ and KZ zones demonstrated the thinning phenomenon.

After the deep drawing process, a maximum effective strain of 0.5 was experienced at the junction (C) of the KZ and FZ regions. The cross-sectional line profile on the deformed part showed that CZ and KZ zones followed a similar trend as stretching process. The transverse strain (ε_{YY}) exhibited a linearly increasing compressive behavior from the start to the end of the FZ region.

Following the spinning process, a maximum effective strain of 2.6 was induced in the FZ region. The effective strain line profile in the FZ region (C-D) showed an increase from 1.15 at point C, reaching a maximum value of 2.45, and then decreasing to 1.92 at the end of the flange path D. The compressive nature of thickness strain (ε_{ZZ}) in the FZ region emphasized the thinning phenomenon.

Acknowledgement

This research was supported by the Basic Science Research Program through the National Research Foundation of Korea (NRF) funded by the Ministry of Education (NRF-2014R1A6A1030419).

REFERENCES

[1] I. Gutierrez-Urrutia, D. Raabe, 2011, Dislocation and twin substructure evolution during strain hardening of an Fe–22 wt.% Mn–0.6 wt.% C TWIP steel observed by electron channeling contrast imaging, Acta Mater., Vol. 59, No. 16, pp. 6449~6462, https://doi.org/10.1016/j.actamat.2011.07.009

[2] Yuhui Wang, Baodong Shi, Yanming He, Hongwang Zhang, Yan Peng and Tiansheng Wang, 2018, A Fine Grain, High-Mn Steel with Excellent Cryogenic Temperature Properties and Corresponding Constitutive Behaviour, Materials, Vol. 11, No. 2. pp. 253~253, https://doi.org/10.3390/ma11020253

[3] Seok Su Sohn, Seokmin Hong, Junghoon Lee, Byeong-Chan Suh, Sung-Kyu Kim, Byeong-Joo Lee, 2015, Effects of Mn and Al contents on cryogenic-temperature tensile and Charpy impact properties in four austenitic high-Mn steels, Acta Mater., Vol. 100, pp. 39~52, http://dx.doi.org/10.1016/j.actamat.2015.08.027

[4] Jia-Kuan Ren, De-shun Mao, Ye Gao, Jun Chen, Zhen-yu Liu, 2021, High carbon alloyed design of a hot-rolled high-Mn austenitic steel with excellent mechanical properties for cryogenic application, Mater. Sci. Eng. A, Vol. 827, pp. 141959~141959, https://doi.org/10.1016/j.msea.2021.141959

[5] International Organization for Standardization 21029-1:2018, Cryogenic vessels-Transportable vacuum insulated vessels of not more than 1000 litres volume - Part 1: Design, fabrication, inspection and tests, ISO 21029-1:2018, Geneva, Switzerland, https://www.iso.org/standard/65433.html

[6] Jinyang Zhenga, Xiangyu Shua, Yingzhe Wua, Huaijian Xua, Qunjie Lua, Binbin Liaoa, Binfeng Zhang, 2018, Investigation on the plastic deformation during the stamping of ellipsoidal heads for pressure vessels, Thin-Walled Struct., Vol. 127, pp. 135~144, https://doi.org/10.1016/j.tws.2018.01.040

[7] H. Soltani, A. Amirat, O. Boussaid, 2019, Contribution in analyzing dimensional deviations in

ellipsoidal steel heads during deep drawing, Int. J. Adv. Manuf. Technol., Vol. 102, No. 5~8, pp. 2451~2463, https://doi.org/10.1007/s00170-018-03270-0

[8] Jinhui Zhang, Mei Zhan, He Yang, Zhiqiang Jiang, Dong Han, 2012, 3D-FE modeling for power spinning of large ellipsoidal heads with variable thicknesses, Comput. Mater. Sci., Vol. 53, No. 1, pp. 303~313, https://doi.org/10.1016/j.commatsci.2011.08.010

[9] G. Totten, M. Howes, T. Inoue, 2002, Handbook of Residual Stress and Deformation of Steel, ASM International, Ohio, United States of America, pp. 144~149.

[10] M.S. Ragab, H.Z. Orban, 2000, Effect of ironing on the residual stresses in deep drawn cups, J. Mater. Process. Technol., Vol. 99, No. 1~3, pp. 54~61, https://doi.org/10.1016/S0924-0136(99)00360-X

[11] Yong-Cheng Lin, Jiang-Shan Zhu, Jia-Yang Chen, Jun-Quan Wang, 2022, Residual-stress relaxation mechanism and model description of 5052H32 Al alloy spun ellipsoidal heads during annealing treatment, Adv. Manuf., Vol. 10, No. 1, pp. 87~100, https://doi.org/10.1007/s40436-021-00367-w

[12] H. W. Swift, 1952, Plastic Instability under Plane Stress, J. Mech. Phys. Solids, Vol. 1, No. 1, pp. 1~18, https://doi.org/10.1016/0022-5096(52)90002-1